Scattering and Pairing in Cuprate Superconductors

Louis Taillefer

Canadian Institute for Advanced Research, Regroupement Québécois sur les Matériaux de Pointe, Département de Physique, Université de Sherbrooke, Sherbrooke, Québec J1K 2R1, Canada; email: Louis.Taillefer@USherbrooke.ca

Annu. Rev. Condens. Matter Phys. 2010. 1:51–70

First published online as a Review in Advance on May 6, 2010

The *Annual Review of Condensed Matter Physics* is online at conmatphys.annualreviews.org

This article's doi: 10.1146/annurev-conmatphys-070909-104117

1947-5454/10/0810-0051$20.00

Key Words

pseudogap phase, quantum critical point, Fermi-surface reconstruction, spin-density-wave order, organic superconductors, pnictide superconductors

Abstract

The origin of the exceptionally strong superconductivity of cuprates remains a subject of debate after more than two decades of investigation. Here we follow a new lead: The onset temperature for superconductivity scales with the strength of the anomalous normal-state scattering that makes the resistivity linear in temperature. The same correlation between linear resistivity and T_c is found in organic superconductors, for which pairing is known to come from fluctuations of a nearby antiferromagnetic phase, and in pnictide superconductors, for which an antiferromagnetic scenario is also likely. In the cuprates, the question is whether the pseudogap phase plays the corresponding role, with its fluctuations responsible for pairing and scattering. We review recent studies that shed light on this phase—its boundary, its quantum critical point, and its broken symmetries. The emerging picture is that of a phase with spin-density-wave order and fluctuations, in broad analogy with organic, pnictide, and heavy-fermion superconductors.

Cuprate: copper oxide material made of layers of CuO_2 in which superconductivity occurs upon either hole or electron doping, with T_c values as high as 164 K or 25 K, respectively

Pnictide: iron-based material made of layers of Fe_2As_2 in which superconductivity can occur, with T_c values as high as 57 K

Pseudogap phase: enigmatic region of the cuprate phase diagram delineated by a crossover temperature T^* below which the electronic density of states is partially gapped

Spin-density wave (SDW): antiferromagnetic modulation of the spin density in a metal; the new periodicity causes a reconstruction of the Fermi surface such that a large hole surface is typically transformed into small electron and hole pockets

Quantum critical point (QCP): point at $T = 0$ in the phase diagram of a material where an ordered phase ends, as a function of pressure, doping, or magnetic field; antiferromagnetic QCPs are found in heavy-fermion, organic, cuprate, and pnictide superconductors

1. INTRODUCTION

Superconductivity is a fascinating, almost magical, property of matter. The ability of a metal to undergo a phase transition and enter a new state of matter in which electrons carry electricity perfectly, with infinite conductivity, sounds like utopia or mathematical fancy. Yet many real materials (such as aluminum, lead, and tin) do have this property of superconductivity. Unfortunately, they do so only at extremely low temperature, near absolute zero. Many modern-day alchemists have dreamt of finding a material with a superconductivity that could survive up to room temperature, at which the wonders of this unique quantum-mechanical state could be exploited more easily. This dream was fueled by the discovery of cuprates in 1986 (1), a family of copper oxide materials in which superconductivity has been found to persist as high as 164 K—halfway to room temperature.

Having stimulated over 100,000 publications, the question of what causes superconductivity in the cuprates is widely considered to be one of the great challenges of condensed-matter physics (2). On the twentieth anniversary of its discovery, it was deemed "a mystery that defies solution" (3). Since then, however, exciting developments have given researchers hope that a solution may in fact be within reach (4). In particular, a new family of superconductors, the pnictides, was discovered (5), with critical temperatures as high as 57 K (6, 7). In this review, I discuss some of the recent developments that shed light on the two major questions of cuprate superconductivity: What causes electron pairing, and what is the nature of the pseudogap phase, the enigmatic region of the phase diagram that overlaps with much of the superconducting phase? I do not attempt to review the field but rather explore a particular perspective, based on the conjecture that the pseudogap phase is fundamentally a phase with spin-density-wave (SDW) order, ending at a quantum critical point (QCP), with its fluctuations dominating the scattering of electrons and their pairing. This would make cuprates similar to heavy-fermion, organic, and pnictide superconductors, for which superconductivity is typically found in close proximity to SDW order. Although many researchers believe that distinct theories are required for the different families of superconductors, I argue here that a fundamentally similar pairing mechanism operates, and this common perspective suggests that a solution may be within reach.

2. PHASE DIAGRAM

The doping phase diagram of hole-doped cuprates is sketched in **Figure 1**. With increased hole concentration (doping) p, the materials go from being antiferromagnetic insulators at zero doping to metals at high doping. Given their density of one electron per Cu in the undoped state, they should be metals even at $p = 0$, with a Fermi surface volume containing $1 + p$ holes; but strong on-site repulsion prevents electron motion and turns the material into a Mott insulator at low doping. At intermediate doping, between the insulator and the metal, there is a central region of superconductivity, delineated by a critical temperature T_c, which can rise to values of order 100 K—higher than in any other family of materials. Near optimal doping, the normal state above T_c is referred to as a strange metal, characterized by a resistivity that is linear in temperature. In the midst of this strange-metal region, the pseudogap phase sets in, below a crossover temperature T^* at which most physical properties undergo a significant change (8). The question is whether the pseudogap phase is a precursor to some hidden ordered state with broken symmetry, or a precursor to the Mott insulator with no broken symmetry. To explore this landscape,

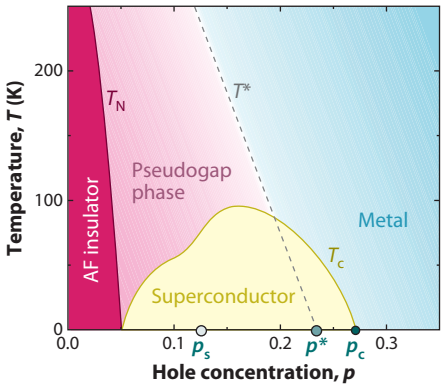

Figure 1

Schematic phase diagram of cuprate superconductors as a function of hole doping p. The Mott insulator at $p = 0$ shows antiferromagnetic (AF) order below T_N, which vanishes rapidly with doping. At high doping, the metallic state shows all the signs of a conventional Fermi liquid. At the critical doping p_c, two events happen simultaneously: Superconductivity appears (below a critical temperature T_c), and the resistivity deviates from its Fermi-liquid behavior, acquiring a linear temperature dependence. The simultaneous onset of T_c and linear resistivity is the starting point for our exploration of cuprates. The evolution from metal to insulator is interrupted by the onset of the pseudogap phase that sets in below a crossover temperature T^*, which goes to zero at a quantum critical point (QCP) located at p^* in the absence of superconductivity (removed, for example, by application of a large magnetic field). The existence, nature, and location of such a QCP are a major focus of this review. In the presence of superconductivity, the QCP may move to lower doping, down to p_S, as a result of a competition between the pseudogap and superconducting phases (9, 10).

we start from the far-right side of **Figure 1**, in the overdoped metallic state. This state is characterized by a large Fermi surface that has a volume containing $1 + p$ holes per Cu atom, as determined by angle-dependent magneto-resistance (11), angle-resolved photoemission spectroscopy (12), and quantum oscillations (13), all performed on the single-layer cuprate $Tl_2Ba_2CuO_{6+\delta}$ (Tl-2201). The low-temperature Hall coefficient R_H of overdoped Tl-2201 is positive and equal to $1 / e\,(1 + p)$ (14), as expected for a single-band metal with a hole density $n = 1 + p$. Conduction in the normal state obeys the Wiedemann-Franz law (15), a hallmark of Fermi-liquid theory. At the highest doping, beyond the superconducting phase (**Figure 1**), the electrical resistivity $\rho(T)$ of Tl-2201 exhibits the standard T^2 temperature dependence of a Fermi liquid (16), also observed in $La_{2-x}Sr_xCuO_4$ (LSCO) (17).

Fermi surface: boundary in k-space that separates occupied electron states from unoccupied states; its volume is directly proportional to the carrier density; when closed, it can be electron-like (enclosing occupied states) or hole-like (enclosing unoccupied states)

Quantum oscillations: oscillations in the resistance or magnetization of a metal as a function of magnetic field B that results from cyclotron motion and Landau quantization of energy levels; their frequency in $1/B$ is proportional to the cross-sectional area of a closed Fermi surface

3. SCATTERING AND PAIRING

The question then is this: What makes superconductivity emerge from this particular, rather conventional, metal? The critical doping at which superconductivity springs is roughly the same in all hole-doped cuprates, namely $p_c \approx 0.27$. Note that although it appears to obey weak-coupling BCS theory, at least initially (15, 18), the superconducting state has d-wave symmetry (19) rather than the usual s-wave symmetry, pointing to an electronic rather than phononic pairing mechanism (20). What happens at p_c to make d-wave pairing prevail? Let us investigate one intriguing clue: At this special doping, the scattering between electrons undergoes a qualitative change. Indeed, it is precisely below p_c

Tl-2201: $Tl_2Ba_2CuO_{6+\delta}$

Fermi liquid: a metal that conforms to Landau's Fermi-liquid theory, with signatures that include a coherent (sharp) Fermi surface, the Wiedemann-Franz law, and a T^2 dependence of the resistivity

LSCO: $La_{2-x}Sr_xCuO_4$

Nd-LSCO: $La_{2-x-y}Nd_ySr_xCuO_4$

that the normal-state electrical resistivity $\rho(T)$ starts to deviate from its quadratic dependence at low temperature (16). At first, $\rho(T)$ acquires an additional linear term, as in Tl-2201 at $p = 0.25$–0.26, where $\rho(T)$ is best described by the form $\rho_0 + AT + BT^2$ below 30 K (14, 15). At slightly lower doping, $\rho(T)$ becomes purely linear, with $\rho(T) = \rho_0 + AT$ below 80 K or so, as found in $La_{1.6-x}Nd_{0.4}Sr_xCuO_4$ (Nd-LSCO) at $p = 0.24$ (21) and LSCO at $p = 0.23$ (22), both measured down to $T \approx 1$ K in a magnetic field large enough to suppress superconductivity (see **Figure 2**). At still lower doping, the linearity of $\rho(T)$ extends to higher temperature, up to 300 K and above. To describe the broad evolution of $\rho(T)$ with doping, available LSCO data (in zero field) (23) were recently fit to the form $\rho(T) = \rho_0 + AT + BT^2$, over a temperature interval from 200 to 400 K (24). The results are shown in **Figure 3**, where the parameter A is plotted versus p; A is seen to extrapolate to zero at $p = 0.27 = p_c$. In other words, $A \to 0$ at the same doping as $T_c \to 0$. Recent high-field measurements on overdoped LSCO show that the same fit performed over an interval from 1 to 200 K provides a good description of the low-temperature data and leads to the same correlation between A and T_c (22). Data on Tl-2201 as $p \to p_c$ (16) yield $A \sim T_c$ (see **Figure 4**). This remarkable correlation between linear resistivity and T_c strongly suggests that anomalous (non-Fermi-liquid) scattering and pairing have a common origin. This correlation is supported by angle-dependent magneto-resistance studies of overdoped Tl-2201 that yield an anisotropic linear-T scattering rate that peaks in the same direction as the d-wave gap (25) and also scales with T_c (26).

Note that the linear resistivity is a universal property of hole-doped cuprates, and different materials exhibit the very same slope (A coefficient) at a given doping, when measured per CuO_2 plane (see 24). In other words, the anomalous scattering is universal, and it switches on at the same doping as superconductivity. The answer to our initial

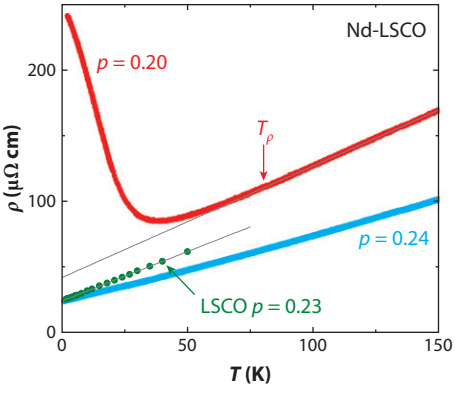

Figure 2

In-plane electrical resistivity of two hole-doped cuprates once superconductivity has been suppressed by application of a sufficiently large magnetic field B: $La_{1.6-x}Nd_{0.4}Sr_xCuO_4$ (Nd-LSCO) at $p = 0.24$ ($B = 33$ T; *blue*) and at $p = 0.20$ ($B = 35$ T; *red*) (data from 21) and $La_{2-x}Sr_xCuO_4$ (LSCO) at $p = 0.23$ ($H = 45$ T; *green*) (data from 22). The data for Nd-LSCO at $p = 0.24$ and LSCO at $p = 0.23$ are both perfectly linear at low temperature, down to at least 1 K. At lower doping, the resistivity of both materials deviates upward from linearity below a certain temperature. This effect is more pronounced in Nd-LSCO, in which it leads to a large upturn, as shown here for $p = 0.20$. T_ρ is the temperature below which the resistivity begins to deviate from its linear dependence at high temperature. Grey lines are linear fits.

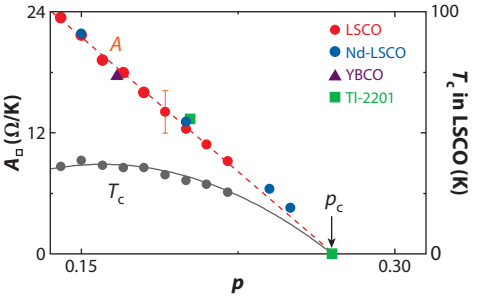

Figure 3

Coefficient of the linear resistivity of cuprates per CuO_2 plane, $A_\square = A / d$, as a function of doping p, for $La_{2-x}Sr_xCuO_4$ (LSCO) (*red dots*; 23, 27), $La_{1.6-x}Nd_{0.4}Sr_xCuO_4$ (Nd-LSCO) (*blue dots*; 21, 28), $YBa_2Cu_3O_y$ (YBCO) (*purple triangle*; 23), and $Tl_2Ba_2CuO_{6+\delta}$ (Tl-2201) (*green squares*; 16, 29). The data are extracted from fits (24) of the form $\rho_0 + AT + BT^2$ to published data. The red dashed line is a linear fit to the LSCO data points. The gray dots are the corresponding T_c for LSCO (23). The gray line is the formula $T_c = T_c^{max}\,[1 - 82.6\,(p - 0.16)^2]$, with $T_c^{max} = 37$ K. Note that the coefficient of the linear term goes to zero at the point at which superconductivity vanishes, i.e., $A \to 0$ as $T_c \to 0$, at $p_c = 0.27$. Figure adapted from Reference 24.

question regarding the cause of *d*-wave pairing would then lie in a second question: What causes the linear temperature dependence of $\rho(T)$ in cuprates? To address this question, we now turn to another family of superconductors, the Bechgaard salts, in which the same correlation between linear resistivity and T_c was recently observed experimentally and elucidated theoretically.

Organic superconductor: material made of stacks of organic molecules that conduct with either 1D or 2D character; superconductivity occurs in both versions, with T_c values of order 1 K and 10 K, respectively

4. ORGANIC AND PNICTIDE SUPERCONDUCTORS

The Bechgaard salts $(TMTSF)_2X$ (X = PF_6, ClO_4) are organic superconductors below $T_c \approx 1$ K (30). Although they display one-dimensional (1D) conduction at high temperature, their conduction is coherent in two dimensions below approximately 100 K. The phase diagram of $(TMTSF)_2PF_6$ under pressure is shown in **Figure 5** (24, 31): An SDW phase gives way to a superconducting phase with increasing pressure. The resistivity of $(TMTSF)_2PF_6$, reproduced in **Figure 6**, exhibits the following salient features (24, 31): (*a*) At a pressure just below the QCP at which SDW order vanishes, $\rho(T)$ undergoes a pronounced upturn at low temperature, upon entering the SDW phase; (*b*) at a pressure just above the QCP, $\rho(T)$ is perfectly linear in temperature down to the lowest temperature; and (*c*) at the highest measured pressure, close to where superconductivity disappears, $\rho(T)$ is quadratic in temperature. These are the three regimes characteristic of a quantum phase transition (at P^*) (32): Fermi-surface reconstruction (and gapping) below P^*, non-Fermi-liquid (*e.g.* linear-T) resistivity at P^*, and recovery of the Fermi-liquid T^2 dependence beyond P^*. Now, the crossover from T to T^2 at $T \to 0$ occurs over an interval of pressure that precisely coincides with the interval over which superconductivity exists (24). In that pressure range, $\rho(T)$ can be fit to the form $\rho_0 + AT + BT^2$, with the A coefficient decreasing monotonically with pressure and scaling with T_c (24, 31), as shown in **Figure 4**. This reveals another instance of the same intimate correlation between linear resistivity and T_c found in the cuprates and highlighted in the previous section.

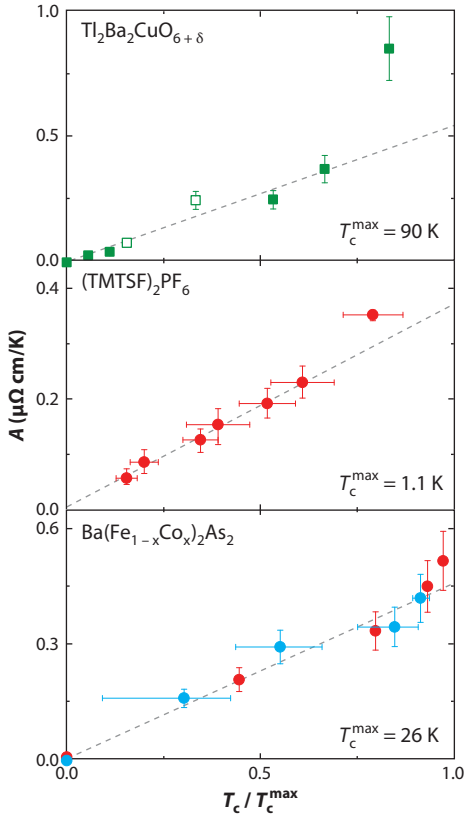

Figure 4

Coefficient of the linear term A in the resistivity $\rho(T)$ as a function of T_c for (*top panel*) the cuprate $Tl_2Ba_2CuO_{6+\delta}$ (Tl-2201) (*closed squares*, data from 16; *open squares*, data from 14, 29), (*middle panel*) the Bechgaard salt $(TMTSF)_2PF_6$ (data from 24, 31), and (*bottom panel*) the pnictide $Ba(Fe_{1-x}Co_x)_2As_2$ (*red dots*, data from 33; *blue dots*, data from 34). The T_c values correspond to different hole dopings, pressures, and cobalt concentrations, respectively, plotted normalized to T_c^{max}, the maximum value of T_c in the phase diagram (as indicated). The A coefficient is obtained from fits of $\rho(T)$ to the form $\rho_0 + AT + BT^2$ (for the *top panel*, see 24; for the *middle and bottom panels*, see 31). Figure adapted from References 24 and 31.

The advantage of the Bechgaard salts is that they are well understood theoretically (30). Weak-coupling renormalization group calculations (35) reproduce the phase diagram—with SDW order giving way to superconductivity—and account in detail for the antiferromagnetic fluctuations observed by nuclear magnetic resonance. This leaves little doubt that pairing and scattering in this material both come from low-energy antiferromagnetic fluctuations. The calculations reveal a fundamental mechanism not considered in previous treatments of non-Fermi-liquid behavior near an antiferromagnetic QCP: the positive interference between pairing correlations and spin fluctuations (24, 31, 35). The pairing correlations enhance the spin fluctuations (35) and thereby impart an anomalous linear temperature dependence to the scattering rate (24, 31), causing the resistivity to deviate from the T^2 dependence expected at $T \to 0$ away from the QCP. This interference

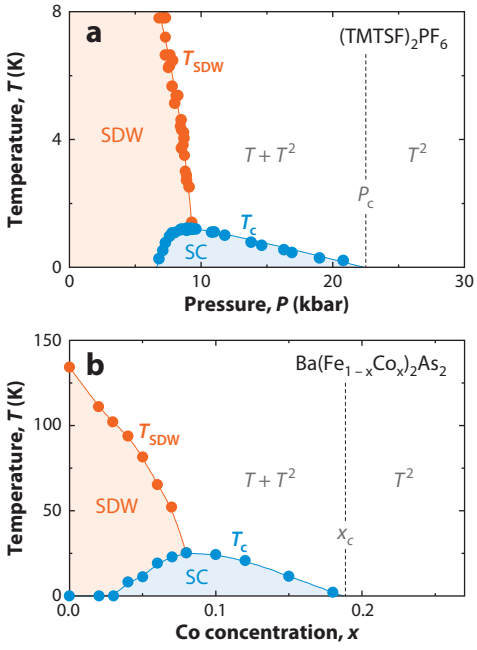

Figure 5

(*a*) Temperature-pressure phase diagram of $(TMTSF)_2PF_6$, showing a spin-density-wave (SDW) phase below T_{SDW} (*orange dots*) and superconductivity (SC) below T_c (*blue dots*) (24, 31). The latter phase ends at the critical pressure P_c. (*b*) Temperature-doping phase diagram of the iron-pnictide superconductor $Ba(Fe_{1-x}Co_x)_2As_2$, as a function of nominal Co concentration x, showing a metallic SDW phase below T_{SDW} and superconductivity below a T_c that ends at the critical doping x_c (33). In both panels, the vertical dashed line separates a regime in which the resistivity $\rho(T)$ grows as T^2 (*on the right-hand side*) from a regime in which it grows as $T + T^2$ (*on the left-hand side*). Figure adapted from Reference 31.

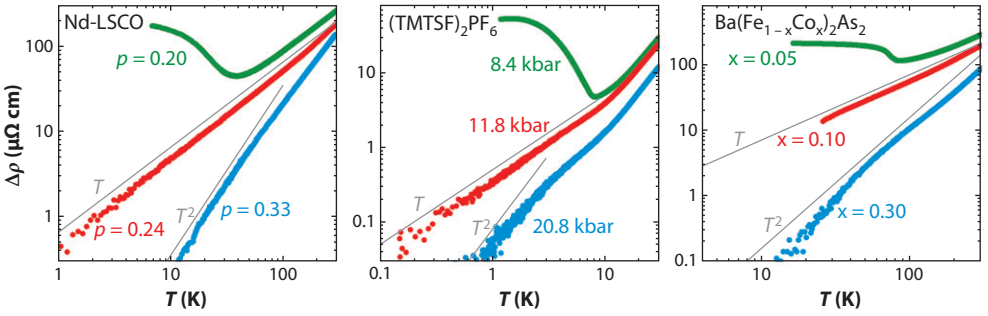

Figure 6

Temperature-dependent part of the in-plane normal-state resistivity of materials in three families of superconductors, plotted as $\rho(T) - \rho_0$ versus T on a log-log scale. Three values of the relevant tuning parameter were chosen: below, at, and above their respective quantum critical points (QCPs). (*Left panel*) Data on hole-doped cuprates $La_{1.6-x}Nd_{0.4}Sr_xCuO_4$ (Nd-LSCO) at $p = 0.20$ and $p = 0.24$ (21) and $La_{2-x}Sr_xCuO_4$ (LSCO) at $p = 0.33$ (17). The QCP at a hole doping $p^* \approx 0.24$ marks the end of the stripe-ordered phase in Nd-LSCO (21, 28). Figure adapted from Reference 36. (*Middle panel*) Data on the organic Bechgaard salt $(TMTSF)_2PF_6$. The QCP at a pressure $P^* \approx 10$ kbar marks the end of the spin-density-wave (SDW) phase. Figure adapted from Reference 31. (*Right panel*) Data on the pnictide $Ba(Fe_{1-x}Co_x)_2As_2$ (33). The QCP at a Co concentration $x^* \approx 0.10$ marks the end of the SDW phase.

mechanism operates as long as pairing correlations are significant, and thus provides a natural explanation for the correlation between anomalous (non-Fermi-liquid) resistivity and T_c. The fact that the same correlation is present in cuprates is strong evidence that the same positive interference is at play: spin fluctuations cause *d*-wave pairing, and *d*-wave correlations enhance scattering. The *d*-wave-like anisotropy of the linear-T scattering detected by angle-dependent magnetoresistance in overdoped Tl-2201 (25) would then be the fingerprint of that interference, the reason why "electrons scatter as they pair" (37).

As non-Fermi-liquid behavior and unconventional superconductivity are but two manifestations of the same interference, the observation of a non-Fermi-liquid resistivity tied to T_c emerges as a smoking gun for pairing mediated by antiferromagnetic spin fluctuations. It is interesting to examine other superconductors in this light. The pnictides are a prime testing ground, given that their phase diagram, shown in **Figure 5** for $Ba(Fe_{1-x}Co_x)_2As_2$, is strikingly similar to that of $(TMTSF)_2PF_6$, with superconductivity peaking at the QCP at which SDW order vanishes. The resistivity of $Ba(Fe_{1-x}Co_x)_2As_2$ (33, 34) shows a linear behavior near the QCP and a purely quadratic dependence as soon as superconductivity disappears (see **Figure 6**). In the intervening regime, $\rho(T)$ can be fit to the form $\rho_0 + AT + BT^2$, with $A \sim T_c$ (24, 31). Pnictides therefore provide a third instance of the same correlation between linear resistivity and T_c (see **Figure 4**). This is strong evidence that the same positive interference between antiferromagnetic spin fluctuations and pairing correlations is at play even though unlike the cuprates and Bechgaard salts, the pairing symmetry of pnictides may not be *d*-wave.

The central organizing principle is the presence of a QCP inside the superconducting dome, at which SDW order ends. This is clearly seen in the organic and pnictide superconductors (**Figure 5**), and in several heavy-fermion superconductors (see sidebar) (20, 32, 38, 39). In the cuprates, the existence, nature, and location of such a QCP are all the subject of debate (40, 41). Below we discuss several experiments that have recently shed light on the question of a QCP in cuprates.

HEAVY-FERMION SUPERCONDUCTORS

Superconductivity was discovered in *f*-electron heavy-fermion materials in 1979 (42), just before its discovery in organic superconductors (43). Strong evidence that pairing in heavy-fermion metals is of antiferromagnetic origin came from the discovery of superconductivity right at the QCP where antiferromagnetic order vanishes with pressure (20, 38). A model of magnetic pairing (20, 44) can account, at least qualitatively, for the 10-fold increase in T_c from cubic $CeIn_3$ (0.2 K) (38) to tetragonal $CeRhIn_5$ (2.3 K) (45), as a result of the enhanced effectiveness of spin-fluctuation pairing in two dimensions. Several heavy-fermion metals exhibit an antiferromagnetic QCP, and non-Fermi-liquid behavior is systematically observed in its vicinity (32), with a sub-quadratic temperature dependence of the resistivity. Whether this non-Fermi-liquid behavior persists away from the QCP, over a range of pressures that coincides with the region of superconductivity, remains to be closely investigated. Existing data on $CeRhIn_5$ (45) suggests that it might. Although the Kondo effect (from the *f* moments), the strong 3D character, and the multi-band Fermi surface all make the problem of scattering and pairing more complex than in the Bechgaard salts, it is not unlikely that antiferromagnetic spin fluctuations play fundamentally the same role, and the quantum-critical behavior is again modified by the positive interference of pairing correlations.

5. QUANTUM CRITICAL POINT AND BROKEN TRANSLATIONAL SYMMETRY

Eu-LSCO: $La_{2-x-y}Eu_ySr_xCuO_4$

Stripe order: unidirectional spin or charge density-wave order; it breaks translational and rotational symmetries; both spin and charge stripes are seen in Nd-LSCO and Eu-LSCO, only spin stripes have so far been seen in YBCO and LSCO

Figure 6 shows that Nd-LSCO exhibits the same three regimes of quantum criticality that are seen in the organic and pnictide superconductors, in which they are associated with an SDW QCP. The upturn in $\rho(T)$ at $p = 0.20$ below 40 K (**Figures 2** and **6**) is caused by a reconstruction of the Fermi surface, as confirmed by a parallel upturn in the Hall (21) and Seebeck (36) coefficients. Although $R_H(T \to 0)$ is consistent with a single large hole-like Fermi surface at $p = 0.24$, being equal to $1/e\,(1 + p)$, it suddenly becomes much larger at $p = 0.20$ and then much smaller (almost negative) at $p = 0.12$ (46). A similar evolution is observed in the Seebeck coefficient S, whereby S/T at $T \to 0$ goes from small positive at $p = 0.24$ to large positive at $p = 0.20$ (36), and then to large negative at $p = 0.12$ (46, 47). These dramatic changes in R_H and S are typical of a Fermi surface that changes topology with doping and includes both hole-like and electron-like portions. In Nd-LSCO and the closely related Eu-doped LSCO (Eu-LSCO), the mechanism responsible for the reconstruction of the large Fermi surface is clear (48): It is the onset of stripe order, a form of SDW order first detected by neutron diffraction (49), with an associated charge-density-wave order (49), also detected by X-ray diffraction (50) and nuclear quadrupole resonance (51). **Figure 7** shows how in Eu-LSCO at $p = 1/8$ the onset of stripe order coincides with the drop in $R_H(T)$ (52), which also coincides with the drop in S/T (47). As shown in the phase diagram of **Figure 8**, the onset of stripe order in Nd/Eu-LSCO occurs at a temperature T_{CO}, which peaks at $p = 1/8$ and decreases monotonically with doping, extrapolating to zero at $p \approx 0.24$. The stripe phase is most stable at 1/8 because at that doping its period is commensurate with that of the lattice (28, 51).

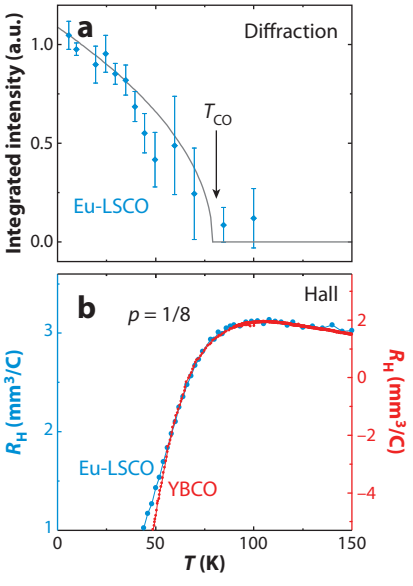

Figure 7

(*a*) Temperature dependence of charge stripe order in Eu-doped LSCO (Eu-LSCO) at $p = 1/8$, as detected by resonant soft X-ray diffraction (data from 53). The grey line is a guide to the eye. (*b*) Hall coefficient versus temperature measured in $B = 15$ T for Eu-LSCO (*blue*, *left axis*; 52) and $YBa_2Cu_3O_y$ (YBCO) (*red*, *right axis*; 54), both at $p \approx 1/8$. Figure adapted from Reference 48.

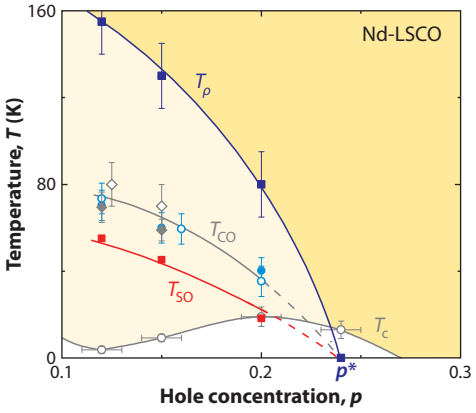

Figure 8

Temperature-doping phase diagram of $La_{1.6-x}Nd_{0.4}Sr_xCuO_4$ (Nd-LSCO) showing the superconducting phase below T_c (*open gray circles*) and the pseudogap region delineated by the crossover temperature T_ρ (*dark blue squares*). Also shown is the region in which magnetic order is observed below T_{SO} (*red squares*) and charge order is detected below T_{CO} (*gray diamonds and light blue circles*). These onset temperatures are respectively defined as the temperatures below which the resistance is zero (21, 28); the in-plane resistivity $\rho(T)$ deviates from its linear dependence at high temperature (21, 28); magnetic Bragg peaks are observed in neutron diffraction (28); and charge order is detected by either X-ray diffraction [Nd-LSCO, *closed gray diamonds* (55); Eu-LSCO, *open gray diamonds* (53)] or nuclear quadrupole resonance [Nd-LSCO, *closed light blue circles*; Eu-LSCO, *open light blue circles* (51)]. Figure adapted from Reference 48.

STM: scanning tunneling microscopy

Therefore, the QCP in Nd-LSCO marks the onset of a finite-$\boldsymbol{Q}$ modulation of the spin and charge densities at $T = 0$ that breaks the translational symmetry of the lattice and hence causes a reconstruction of the Fermi surface. (It is possible that spin and charge order set in at somewhat different dopings and temperatures.) The critical doping at which this symmetry-breaking and Fermi-surface reconstruction occur was pinpointed by tracking the upturn in the *c*-axis resistivity of Nd-LSCO (56), giving $p^* = 0.235 \pm 0.005$. A similar study performed on $Bi_2Sr_2CaCu_2O_{8+\delta}$ gave a comparable value of p^* (57). Calculations (58) show that stripe order does cause the Fermi surface to break up into small electron and hole pockets (plus some quasi-1D sheets), and these can give rise to positive and negative swings in $R_H(T \to 0)$ as the SDW potential grows with underdoping (59).

This establishes the existence of a QCP inside the superconducting dome, at which stripe order (a form of SDW order) ends, much as in the organic and pnictide superconductors. The analogy then suggests that fluctuations of the stripe order are responsible for the linear resistivity and, given the correlation with T_c, the pairing. In support of this connection, the strength of antiferromagnetic fluctuations in overdoped LSCO measured by inelastic neutron scattering has been shown to scale with T_c (60). Two important questions now arise: Is stripe order a generic property of hole-doped cuprates? Is the pseudogap phase related to stripe order? We address the first question in the remainder of this section and explore the second question in Section 6.

Scanning tunneling microscopy (STM) studies have revealed real-space modulations of the charge density in three different hole-doped cuprates (61–65): $Bi_2Sr_2CaCu_2O_{8+\delta}$, $Ca_{2-x}Na_xCuO_2Cl_2$, and $Bi_2Sr_2CuO_{6+x}$. These have stripe-like unidirectional character on the nanometer scale (64, 66). The modulations persist into the overdoped regime, and

their real-space period appears to lengthen with doping (63), which points to a charge-density-wave order driven by Fermi-surface nesting. Neutron scattering studies have revealed stripe-like SDW order in LSCO for dopings below $p_S \approx 1/8$ (67). This critical doping moves up in a magnetic field (67, 68), such that the QCP is expected to be roughly at $p^* \approx 0.2$ once superconductivity has been fully suppressed. The fact that the QCP moves up with field, from p_S in the superconducting state up to p^* in the normal state (see **Figure 1**), is attributed to a competition between SDW and superconducting phases (9, 10, 69). In Nd-LSCO, in which stripe order is stronger, the presence of a weakened superconductivity has little effect on p^*, and hence $p_S \approx p^* = 0.235$. In LSCO, superconductivity is stronger, and its presence does shift the QCP down significantly. Taken together, STM, neutron, and X-ray studies on several different materials make a strong case that stripe order is a generic tendency of hole-doped cuprates at low temperature (for reviews on stripe order and fluctuations, see 70 and 71).

Because of its high maximal T_c and low level of disorder, the case of $YBa_2Cu_3O_y$ (YBCO) deserves special attention; any phenomenon deemed generic should be seen in YBCO. Muon spin relaxation has shown that magnetism is present in YBCO below $p \approx 0.08$ (72), and neutron diffraction has revealed SDW order in YBCO, but again only up to $p \approx 0.08$ (73). Although it is quite conceivable that in zero field the SDW phase is confined to such low doping because of a particularly strong competition from superconductivity (see 74), it is important to establish whether SDW order persists up to higher doping in the absence of such competition. A number of recent studies in high magnetic fields provide compelling evidence that it does.

The observation of quantum oscillations in YBCO at $p = 0.10$–0.11 (75, 76) revealed the existence of a small closed pocket in the Fermi surface of an underdoped cuprate at $T \to 0$ (see **Figure 9**), whose k-space area is some 30 times smaller than the area enclosed by the large hole-like cylinder characteristic of the overdoped regime (13). Similar oscillations were also observed in $YBa_2Cu_4O_8$, for which $p \approx 0.14$ (77, 78). The fact that the Hall coefficient of both materials is large and negative at $T \to 0$ (see **Figure 10**) indicates that

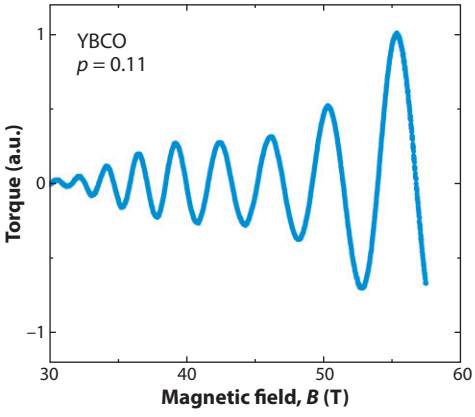

Figure 9

Quantum oscillations in the magnetization of $YBa_2Cu_3O_y$ (YBCO) at $p = 0.11$, detected by torque magnetometry as a function of magnetic field B at $T = 0.7$ K (data from 79). Such quantum oscillations were first observed in the resistance of YBCO at $p = 0.10$ (75) (see **Figure 10**). They come from electron orbits around a small closed pocket in the Fermi surface of this underdoped cuprate in its ground state, once superconductivity has been suppressed by the field.

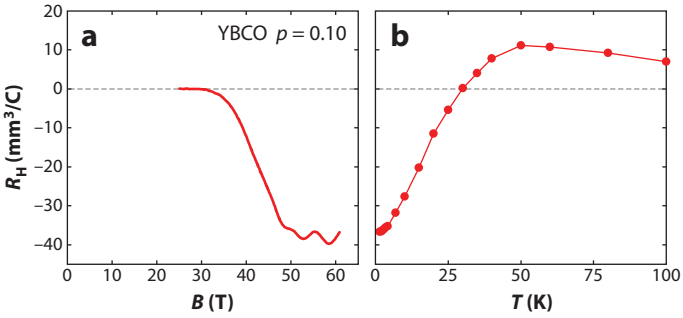

Figure 10

Hall coefficient of $YBa_2Cu_3O_y$ (YBCO) at $p = 0.1$ (*a*) as a function of magnetic field B at $T = 1.5$ K and (*b*) as a function of temperature at $B = 55$ T (data from 54). The fact that quantum oscillations are observed on a large negative background implies that they arise from orbits around a closed electron-like Fermi surface pocket, as confirmed by a negative Seebeck coefficient (47). Figure adapted from Reference 48.

this small closed Fermi pocket is in fact electron-like (54). The normal-state Seebeck coefficient reaches a negative value of S/T as $T \to 0$, which is quantitatively consistent with the frequency and cyclotron mass of the quantum oscillations only if those come from an electron Fermi pocket (47). The very existence of an electron pocket in a hole-doped cuprate is compelling evidence of broken translational symmetry, the result of a Fermi-surface reconstruction caused by the onset of some new periodicity (80). In YBCO at $p = 0.12$, $R_H(T)$ starts its descent to negative values upon cooling in precisely the same way as it does in Eu-LSCO at $p = 0.125$ (48), for which this drop is associated unambiguously with the onset of stripe order (see **Figure 7**). The same striking similarity between YBCO and Eu-LSCO is observed in the way that S/T falls to negative values (47), pointing again to the same underlying mechanism, the onset of stripe order. In YBCO, this mechanism is still present at $p \approx 0.14$, and extrapolation suggests that $p^* > 0.2$. Taken together, these high-field data support the case that the normal-state QCP identified in Nd-LSCO at $p^* = 0.235$ is also present in YBCO and is therefore a generic property of hole-doped cuprates, once the competing superconducting phase has been removed.

Note that the temperature below which Fermi-surface reconstruction in YBCO begins (i.e., where R_H and S/T start to fall) is maximal at $p = 1/8$ (54), the doping at which T_c is most strongly suppressed relative to its ideal parabolic dependence on doping (81). The fact that the peak (in R_H maximum) and dip (in T_c) coincide is consistent with a scenario of competing stripe and superconducting orders, the former being stabilized by commensurate locking with the lattice at $p = 1/8$, as in the La_2CuO_4-based cuprates. Note also that the electron-pocket state is not induced by the magnetic field: At $p = 1/8$, the drop in $R_H(T)$ is observed in the limit of zero field and is independent of field (54, 82). The field simply serves to remove superconductivity and allow transport measurements to be extended to the $T \to 0$ limit.

6. PSEUDOGAP PHASE AND BROKEN ROTATIONAL SYMMETRY

Above we focus on the $T \to 0$ limit and argue that there is a generic normal-state QCP in the overdoped regime of hole-doped cuprates, below which translational symmetry is broken and the large hole-like Fermi surface is reconstructed. We now examine this same

process as a function of temperature. In other words, after having investigated a p-cut at $T = 0$ in the phase diagram (**Figure 1**), across the QCP at p^*, we now look at a T-cut at $p < p^*$, across the pseudogap temperature T^*.

We begin by defining T^* as the temperature T_ρ below which the in-plane resistivity $\rho(T)$ deviates from its linear temperature dependence at high temperature—a standard definition of T^* in YBCO (8, 83). In Nd-LSCO, T_ρ marks the onset of an upward deviation in $\rho(T)$, which eventually leads to an upturn at low temperature (**Figure 2**). In **Figure 8**, T_ρ is plotted as a function of doping; it goes to zero at p^*. Note that T_{CO}, the onset of long-range stripe order, which also vanishes roughly at p^*, lies well below T_ρ so that $T_\rho \approx 2\ T_{CO}$. This suggests that T_ρ marks the onset of stripe fluctuations and that the pseudogap phase below T^* is initially just a short-range/fluctuating precursor of the order that eventually develops fully at lower temperature (48, 84).

As a probe of electronic transformations and phase transitions, the Nernst effect is in general vastly more sensitive than resistivity (85), in essence because changes in carrier density and scattering rate tend to combine in the former, whereas they tend to cancel in the latter. Nernst measurements have been used only recently to study the onset of the pseudogap phase in cuprates (52, 86, 87). A pseudogap temperature T_ν can be defined from the Nernst coefficient $\nu(T)$ in much the same way as for $\rho(T)$, namely as the temperature below which ν/T deviates from its linear temperature dependence at high temperature (52, 87). The resulting phase diagram is shown in **Figure 11*a*** for LSCO, Eu-LSCO, and Nd-LSCO and in **Figure 11*b*** for YBCO. First, we see that $T_\nu = T_\rho$ within error bars.

Nernst effect: transverse electric field E_y across the width of a metallic sample that develops when a temperature gradient $\partial T / \partial x$ is applied along its length in the presence of a perpendicular magnetic field B; the Nernst coefficient is defined as $\nu = E_y / (B\ \partial T / \partial x)$

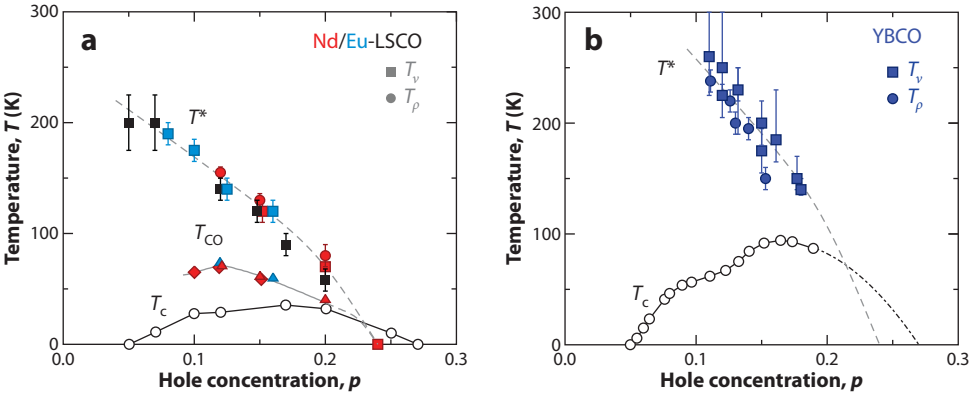

Figure 11

Doping dependence of T_ρ and T_ν, the temperatures below which the resistivity ρ and the Nernst coefficient ν, respectively, deviate from their linear behavior at high temperature, two measures of the pseudogap crossover temperature T^*. (*a*) T_ρ for $La_{1.6-x}Nd_{0.4}Sr_xCuO_4$ (Nd-LSCO) (*red circles*; see **Figure 8**); T_ν for Nd-LSCO (*red squares*; 52), Eu-doped LSCO (Eu-LSCO) (*blue squares*; 52; O. Cyr-Choinière, R. Daou, F. Laliberté, D. LeBoeuf, N. Doiron-Leyraud, et al., submitted manuscript), and $La_{2-x}Sr_xCuO_4$ (LSCO) (*black squares*; obtained in O. Cyr-Choinière, R. Daou, F. Laliberté, D. LeBoeuf, N. Doiron-Leyraud, et al., submitted manuscript, from data in 88). Also shown are the superconducting temperature T_c of LSCO (*open black circles*; 88) and the onset of stripe order in Nd/Eu-LSCO at T_{CO} (*triangles* for nuclear quadrupole resonance and *diamonds* for X-ray diffraction; see **Figure 8**). Figure adapted from O. Cyr-Choinière, R. Daou, F. Laliberté, D. LeBoeuf, N. Doiron-Leyraud, et al., submitted manuscript. (*b*) Equivalent data for $YBa_2Cu_3O_y$ (YBCO), with T_c data from Reference 81. The dashed line is a guide to the eye and is the same dashed line as in panel *a*, multiplied by a factor of 1.5. Figure adapted from Reference 87.

This shows that both ρ and ν detect the same pseudogap temperature T^*, which is not surprising as ν involves the energy derivative of the conductivity (85). Second, T_ν is the same in LSCO and Eu/Nd-LSCO. This shows that the onset of the pseudogap phase is independent of the detailed crystal structure and the relative strength of stripe order and superconductivity. It also strongly suggests that the elusive normal-state QCP in LSCO (22) is located at the same doping p^* as it is in Nd-LSCO (namely at $p \approx 0.24$), or close to it. Thirdly, T_ν in YBCO can be tracked all the way up to $p = 0.18$ (87), the highest doping achievable in pure YBCO [at full oxygen content (81)]. Comparison with the LSCO phase diagram suggests that T_ν in YBCO will extrapolate to zero at much the same p^*. This is further support for a generic normal-state QCP in hole-doped cuprates at $p^* \approx 0.24$.

The suggestion that T^* marks the onset of stripe fluctuations (or short-range order) has recently received strong support from a study of the Nernst effect in untwinned crystals of YBCO (87). Measurements with the temperature gradient applied along the a axis and then the b axis of the orthorhombic lattice reveal a pronounced anisotropy that grows with decreasing temperature, starting precisely at T^* throughout the phase diagram and reaching values as high as $\nu_b / \nu_a = 7$ before superconductivity intervenes (87) (see **Figure 12**). These findings are consistent with prior evidence of in-plane anisotropy in the resistivity (89) and in the spin fluctuation spectrum (73), detected below $p \approx 0.08$. The Nernst data now provide the missing link to the pseudogap

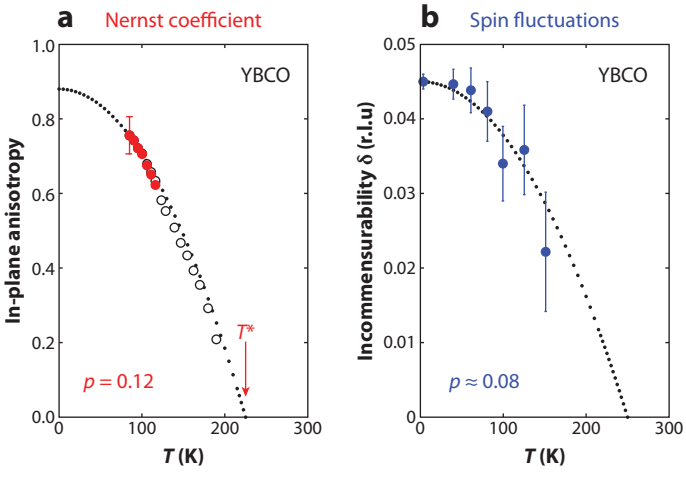

Figure 12

(*a*) *a-b* anisotropy ratio of the Nernst coefficient ν of $YBa_2Cu_3O_y$ (YBCO) at $p = 0.12$, plotted as $(\nu_b - \nu_a) / (\nu_b + \nu_a)$ (*red circles*) and $[D(T) - D(T_\nu)] / [S(T) - S(T_\nu)]$ (*open circles*) versus T, where $D(T) \equiv (\nu_a - \nu_b) / T$ and $S(T) \equiv - (\nu_a + \nu_b) / T$. The anisotropy grows with decreasing temperature, starting right at the pseudogap temperature T^* (defined from T_ν) for all dopings (see 87). It shows that the pseudogap phase breaks the rotational symmetry of the CuO_2 planes (87). Figure adapted from Reference 87. (*b*) Incommensurability (in reciprocal lattice units) of the spin fluctuation spectrum measured in YBCO at $p \approx 0.08$ by inelastic neutron scattering (data from 73). This incommensurability is anisotropic, observed only along the a^* axis. It reveals the appearance of unidirectional character in the spin-density-wave fluctuations below T^*.

phase by showing that T^* marks the onset of broken rotational symmetry in the electronic properties of the CuO_2 planes. This unidirectional character is one of the defining signatures of stripe order (70, 71, 84). Microwave and STM studies have provided complementary evidence of broken rotational symmetry, observed at low temperature in the superconducting state. The microwave conductivity of YBCO exhibits a strong in-plane anisotropy at $p = 0.1$, which is not present at $p = 0.18$ (90), suggesting that the zero-field QCP in YBCO lies between those two dopings, i.e., $0.1 < p_S < 0.18$ (see **Figure 1**). STM revealed that rotational symmetry is broken on the local scale at the surface of two cuprates (64, 66), in the simultaneous presence of broken translational symmetry (66). This glassy nanostripe order has been linked to the pseudogap energy scale (91).

In summary, the following picture of the pseudogap phase is emerging. All hole-doped cuprates have a similar T^* line that ends at a universal critical point p^*, near 0.24 in the absence of superconductivity. Below this normal-state QCP, the large hole-like Fermi surface characteristic of the overdoped regime is reconstructed into several pieces, including electron-like pockets and hole-like sheets. This reconstruction is caused by the onset of stripe order, which breaks the translational symmetry of the lattice at low temperature. With increasing temperature, the stripe-ordered phase ends well before the pseudogap crossover temperature T^*; the intervening region of the phase diagram is most likely a regime of fluctuating short-range stripe order, which breaks the fourfold rotational symmetry of the lattice. Just to the right of the T^* line, and down to $T = 0$ at p^*, the resistivity is linear in temperature; the scattering mechanism responsible for this non-Fermi-liquid behavior is most likely the fluctuations of the pseudogap phase, i.e., stripe fluctuations. The intimate connection between linear resistivity and T_c strongly suggests that scattering and pairing have a common origin, rooted in the fluctuations of the ordered phase, a type of SDW order.

7. ELECTRON-DOPED CUPRATES

Above we only consider hole-doped cuprates. We now turn to the electron-doped cuprates (for a recent review of electron-doped cuprates, see 92). The picture that has emerged over the past few years on that side of the phase diagram is remarkably similar to what is summarized in the last section. This section lists the key findings, obtained mostly from two materials, $Pr_{2-x}Ce_xCuO_4$ and $Nd_{2-x}Ce_xCuO_4$. The pseudogap crossover temperature T^* decreases with x and vanishes at a critical electron doping $x^* \approx 0.17$ (92). Moreover, from the Hall effect data in the $T \to 0$ limit (93), there is a normal-state QCP at $x^* = 0.165 \pm 0.005$, below which the large hole-like Fermi surface is reconstructed into small electron and hole pockets. This reconstructed topology is confirmed by angle-resolved photoemission spectroscopy (94), from which both electron and hole pockets have been seen. The transition from small to large Fermi surface was recently detected via quantum oscillation measurements across x^* (95). The observed reconstruction can be accounted for in a model of commensurate SDW (antiferromagnetic) order, which breaks the translational symmetry of the lattice below x^* (96). Long-range antiferromagnetic order has been observed by neutron scattering to set in below a temperature T_N that appears to vanish at a critical doping somewhat lower than x^*, namely $x \approx 0.13$ (97). The separation between this zero-field onset of antiferromagnetic order and the in-field normal-state

QCP at x^* may again result from the competing effect of superconductivity (9). Additionally, T^* lies significantly above T_N, with $T^* \approx 2\ T_N$; because T^* is roughly the temperature below which the antiferromagnetic correlation length exceeds the thermal de Broglie wavelength of the charge carriers (97), the pseudogap phase has been interpreted (98) as a regime of short-range antiferromagnetic correlations (the so-called renormalized classical regime). Finally, the resistivity exhibits the three regimes of quantum criticality (93): perfectly linear in temperature down to the lowest temperature at x^* (99); upturn at low temperature for $x < x^*$; and curvature, approaching T^2, for $x > x^*$.

The same basic scenario invoked for the hole-doped side applies here on the electron-doped side, with a QCP as the central organizing principle. Below that QCP, there is SDW order, broken translational symmetry, and Fermi-surface reconstruction. Coming down in temperature, a two-stage evolution occurs in which short-range SDW correlations/fluctuations appear first below T^* and long-range order only sets in later. That the SDW order is commensurate with wavevector $\boldsymbol{Q} = (\pi, \pi)$ means that the fourfold rotational symmetry of the lattice is not broken in this case. At the QCP, at which T_c peaks (in zero field), the resistivity is perfectly linear, almost certainly the result of scattering by antiferromagnetic fluctuations. (A linear resistivity as $T \to 0$ has only ever been observed on the border of antiferromagnetic order.) There is only one missing piece to complete the mirror-like symmetry of the phenomena on both sides of the cuprate phase diagram: a correlation between linear resistivity and T_c in the electron-doped materials. I predict that this correlation will be found there too.

8. CONCLUSION

Stepping back to look at the high-T_c puzzle from a distance, incorporating both sides of the cuprate phase diagram and bearing in mind the broad landscape of unconventional superconductivity as we have come to know it over the past 30 years, the essential ingredient appears to be a QCP at which SDW order comes to an end. Associated with this QCP are antiferromagnetic spin fluctuations that can mediate anisotropic pairing and scatter electrons in a way that is in turn strongly influenced by the pairing correlations. The intimate connection between pairing and scattering observed in organic, pnictide, and cuprate superconductors is the tell-tale sign that antiferromagnetism and superconductivity work hand in hand in those materials. This positive interference between spin fluctuations and pairing correlations is a new avenue to be explored in our quest for a room-temperature superconductor.

SUMMARY POINTS

1. There is a QCP in both hole-doped and electron-doped cuprates at which the large hole-like Fermi surface of the overdoped regime is reconstructed.
2. The reconstructed Fermi surface is typically made of both small electron pockets and other hole-like surfaces. This reconstruction affects all electronic properties of these materials, including their ability to form a superconducting state.

3. The reconstruction is caused by the spontaneous onset of a new spatial periodicity that breaks the translational symmetry of the lattice. The order is most likely commensurate antiferromagnetism on the electron-doped side and stripe order—a form of unidirectional and generally incommensurate SDW—on the hole-doped side. Stripe order also breaks the rotational symmetry of the tetragonal CuO_2 planes.
4. The pseudogap temperature T^* marks the onset of antiferromagnetic correlations in electron-doped cuprates and the onset of a strong in-plane anisotropy in the transport properties of hole-doped cuprates, most likely because of anisotropic spin fluctuations.
5. The QCP is the end of the pseudogap boundary, at which the crossover temperature T^* goes to zero. It is located inside the region of superconductivity in the phase diagram.
6. Right at the QCP, in both electron- and hole-doped cuprates, the resistivity is perfectly linear in temperature as $T \to 0$. Only ever observed on the border of SDW order, such a linear resistivity is attributed to the scattering of charge carriers by antiferromagnetic spin fluctuations near a QCP.
7. A linear resistivity as $T \to 0$ was recently observed in both organic and pnictide superconductors, again on the border of SDW order.
8. The strength of this linear resistivity is found to scale with T_c in cuprate, organic, and pnictide superconductors. This direct empirical correlation strongly suggests that pairing and linear-T scattering have a common origin, most likely antiferromagnetic spin fluctuations in all three families of materials.

FUTURE ISSUES

1. Why is the T_c of cuprates higher on the hole-doped side?
2. Why does the electron system in cuprates have a preference for unidirectional incommensurate order on the hole-doped side?
3. Is charge order in hole-doped cuprates fundamental or simply secondary to spin order?
4. How does the underdoped metal, with a Fermi surface that is still coherent at $p = 0.1$, turn into a Mott insulator as $p \to 0$?
5. Is the positive interference between pairing correlations and spin fluctuations, discovered in studies of organic superconductors, a general mechanism for non-Fermi-liquid behavior near an antiferromagnetic QCP?

DISCLOSURE STATEMENT

The author is not aware of any affiliations, memberships, funding, or financial holdings that might be perceived as affecting the objectivity of this review.

ACKNOWLEDGMENTS

I would like to thank Kamran Behnia, Claude Bourbonnais, Andrey Chubukov, Nicolas Doiron-Leyraud, Richard Greene, Catherine Kallin, Steve Kivelson, Gilbert Lonzarich, Andrew Millis, Michael Norman, Cyril Proust, Subir Sachdev, André-Marie Tremblay, and Matthias Vojta for helpful discussions. I would like to acknowledge the support of the Canadian Institute for Advanced Research and funding from NSERC, FQRNT, CFI, and a Canada Research Chair.

LITERATURE CITED

1. Bednorz JG, Muller KA. 1986. *Z. Phys. B Condens. Matter* 64:189–93
2. Committee on CMMP 2010, Solid State Sciences Committee, National Research Council. *Condensed-Matter and Materials Physics: The Science of the World Around Us*. Washington, DC: Nat. Acad. Press. 284 pp.
3. Cho A. 2006. *Science* 314:1072–75
4. Chu CW. 2009. *Nat. Phys.* 5:787–79
5. Kamihara Y, Watanabe T, Hirano M, Hosono H. 2008. *J. Am. Chem. Soc.* 130:3296–97
6. Ishida K, Nakai Y, Hosono H. 2009. *J. Phys. Soc. Jpn.* 78:062001
7. Day C. 2009. *Phys. Today* 62:36–40
8. Timusk T, Statt B. 1999. *Rep. Prog. Phys.* 62:61–122
9. Sachdev S. 2010. *Phys. Status Solidi b*. In press
10. Moon EG, Sachdev S. 2009. *Phys. Rev. B* 80:035117
11. Hussey NE, Abdel-Jawad M, Carrington A, Mackenzie AP, Balicas L. 2003. *Nature* 425:814–17
12. Platé M, Mottershead JDF, Elfimov IS, Peets DC, Liang R, et al. 2005. *Phys. Rev. Lett.* 95:077001
13. Vignolle B, Carrington A, Cooper RA, French MMJ, Mackenzie AP, et al. 2008. *Nature* 455:952–55
14. Mackenzie AP, Julian SR, Sinclair DC, Lin CT. 1996. *Phys. Rev. B* 53:5848–55
15. Proust C, Boaknin E, Hill RW, Taillefer L, Mackenzie AP. 2002. *Phys. Rev. Lett.* 89:147003
16. Manako T, Kubo Y, Shimakawa Y. 1992. *Phys. Rev. B* 46:11019
17. Nakamae S, Behnia K, Mangkorntong N, Nohara M, Takagi H, et al. 2003. *Phys. Rev. B* 68:100502
18. Hawthorn DG, Li SY, Sutherland M, Boaknin E, Hill RW, et al. 2007. *Phys. Rev. B* 75:104518
19. Tsuei CC, Kirtley JR. 2000. *Rev. Mod. Phys.* 72:969–1016
20. **Monthoux P, Lonzarich GG, Pines D. 2007. *Nature* 450:1177**
21. Daou R, Doiron-Leyraud N, LeBoeuf D, Li SY, Laliberté F, et al. 2009. *Nat. Phys.* 5:31–34
22. Cooper RA, Wang Y, Vignolle B, Lipscombe OJ, Hayden SM, et al. 2009. *Science* 323:603–7
23. Ando Y, Komiya S, Segawa K, Ono S, Kurita Y. 2004. *Phys. Rev. Lett.* 93:267001
24. Doiron-Leyraud N, Auban-Senzier P, René de Cotret S, Sedeki A, Bourbonnais C, et al. 2009. arXiv:0905.0964
25. Abdel-Jawad M, Kennett MP, Balicas L, Carrington A, Mackenzie AP, et al. 2006. *Nat. Phys.* 2:821–25
26. Abdel-Jawad M, Analytis JG, Balicas L, Carrington A, Charmant JPH, et al. 2007. *Phys. Rev. Lett.* 99:107002
27. Boebinger GS, Ando Y, Passner A, Kimura T, Okuya M, et al. 1996. *Phys. Rev. Lett.* 77:5417–20
28. Ichikawa N, Uchida S, Tranquada JM, Niemöller T, Gehring PM, et al. 2000. *Phys. Rev. Lett.* 85:1738–41
29. Tyler AW, Ando Y, Balakirev FF, Passner A, Boebinger GS, et al. 1998. *Phys. Rev. B* 57:728–31
30. **Bourbonnais C, Jérome D. 2008. In *The Physics of Organic Superconductors and Conductors*, ed. A Lebed, Vol. 110. New York: Springer. 754 pp.**

20. Distills the essence of a theoretical framework from which superconductivity on the border of ferromagneic and antiferromagnetic instabilities can be understood.

30. Describes how weak-coupling renormalization group calculations can reproduce the phase diagram of the Bechgaard salts, finding that superconductivity follows naturally from SDW order, being mediated by antiferromagnetic spin fluctuations.

31. Doiron-Leyraud N, Auban-Senzier P, René de Cotret S, Bourbonnais C, Jérome D, et al. 2009. *Phys. Rev. B* 80:214531
32. v. Löhneysen H, Rosch A, Vojta M, Wölfle P. 2007. *Rev. Mod. Phys.* 79:1015–75
33. Fang L, Luo H, Cheng P, Wang Z, Jia Y, et al. 2009. *Phys. Rev. B* 80:140508
34. Chu J-H, Analytis JG, Kucharcyk C, Fisher IR. 2009. *Phys Rev. B* 79:014506
35. Bourbonnais C, Sedeki A. 2009. *Phys. Rev. B* 80:085105
36. Daou R, Cyr-Choinière O, Laliberté F, LeBoeuf D, Doiron-Leyraud N, et al. 2009. *Phys. Rev. B* 79:180505
37. Taillefer L. 2006. *Nat. Phys.* 2:809–10
38. Mathur N, Grosche FM, Julian SR, Walker IR, Freye DM, et al. 1998. *Nature* 394:39–43
39. Pham LD, Park T, Maquilon S, Thompson JD, Fisk Z. 2006. *Phys. Rev. Lett.* 97:056404
40. Norman MR, Pines D, Kallin C. 2005. *Adv. Phys.* 54:715–33
41. Broun DM. 2008. *Nat. Phys.* 4:170–72
42. Steglich F, Aarts J, Bredl CD, Lieke W, Meschede D, et al. 1979. *Phys. Rev. Lett.* 43:1892–96
43. Jérome D, Mazaud A, Ribault M, Bechgaard K. 1980. *J. Phys. Lett.* 41:L95–98
44. Monthoux P, Lonzarich GG. 2002. *Phys. Rev. B* 66:224504
45. Park T, Sidorov VA, Ronning F, Zhu J-X, Tokiwa Y, et al. 2008. *Nature* 456:366–68
46. Nakamura Y, Uchida S. 1992. *Phys. Rev. B* 46:5841–44
47. Chang J, Daou R, Proust C, LeBoeuf D, Doiron-Leyraud N, et al. 2010. *Phys. Rev. Lett.* 104:057005
48. Taillefer L. 2009. *J. Phys. Condens. Matter* 21:164212
49. Tranquada JM, Sternlieb BJ, Axe JD, Nakamura Y, Uchida S. 1995. *Nature* 375:561–63
50. Zimmermann MV, Vigliante A, Niemöller T, Ichikawa N, Frello T, et al. 1998. *Europhys. Lett.* 41:629–34
51. Hunt AW, Singer PM, Cederström AF, Imai T. 2001. *Phys. Rev. B* 64:134525
52. Cyr-Choinière O, Daou R, Laliberté F, LeBoeuf D, Doiron-Leyraud N, et al. 2009. *Nature* 458:743–45
53. Fink J, Schierle E, Weschke E, Geck J, Hawthorn D, et al. 2009. *Phys. Rev. B* 79:100502
54. LeBoeuf D, Doiron-Leyraud N, Levallois J, Daou R, Bonnemaison J-B, et al. 2007. *Nature* 450:533–36
55. Niemöller T, Ichikawa N, Frello T, Hünnefeld H, Andersen NH, et al. 1999. *Eur. Phys. J. B* 12:509–13
56. Cyr-Choinière O, Daou R, Chang J, Laliberté F, Doiron-Leyraud N, et al. 2010. *Phys. C.* In press. doi:10.1016/j.physc.2009.11.073
57. Murata K, Kushibiki H, Watanabe T, Kudo K, Nishizaki T, et al. 2010. *Phys. C.* In press. doi:10.1016/j.physc.2010.01.027
58. Millis AJ, Norman MR. 2007. *Phys. Rev. B* 76:220503
59. Lin J, Millis AJ. 2008. *Phys. Rev. B* 78:115108
60. Wakimoto S, Zhang H, Yamada K, Swainson I, Kim H, Birgeneau RJ. 2004. *Phys. Rev. Lett.* 92:217004
61. Vershinin M, Misra S, Ono S, Abe Y, Ando Y, Yazdani A. 2004. *Science* 303:1995–98
62. Hanaguri T, Lupien C, Kohsaka Y, Lee D-H, Azuma M, et al. 2004. *Nature* 430:1001–5
63. Wise WD, Boyer MC, Chatterjee K, Kondo T, Takeuchi T, et al. 2008. *Nat. Phys.* 4:696–99
64. Howald C, Eisaki H, Kaneko N, Greven M, Kapitulnik A. 2003. *Phys. Rev. B* 67:014533
65. Hoffman JE, Hudson EW, Lang KM, Madhavan V, Eisaki H, et al. 2002. *Science* 295:466–69
66. Kohsaka Y, Taylor C, Fujita K, Schmidt A, Lupien C, et al. 2007. *Science* 315:1580–85
67. Chang J, Niedermayer Ch, Gilardi R, Christensen NB, Rønnow HM, et al. 2008. *Phys. Rev. B* 78:104525
68. Khaykovich B, Wakimoto S, Birgeneau RJ, Kastner MA, Lee YS, et al. 2005. *Phys. Rev. B* 71:220508
69. Demler E, Sachdev S, Zhang Y. 2001. *Phys. Rev. Lett.* 87:067202
70. Vojta M. 2009. *Adv. Phys.* 58:564–685

32. Describes the non-Fermi-liquid behavior found in the vicinity of a magnetic quantum critical point and the models proposed to account for it, with examples mostly from heavy-fermion metals.

38. Presents the first observation of superconductivity appearing at an antiferromagnetic QCP in two heavy-fermion metals that also display a non-Fermi-liquid temperature dependence of the resistivity.

40. Presents an overview of the properties of the pseudogap phase in cuprates and the theoretical scenarios proposed to account for that phase.

70. Presents a recent and comprehensive review of the experimental evidence for stripe order in cuprates.

71. Kivelson SA, Bindloss IP, Fradkin E, Oganesyan V, Tranquada JM, et al. 2003. *Rev. Mod. Phys.* 75:1201–41
72. Sanna S, Allodi G, Concas G, Hillier AD, De Renzi R. 2004. *Phys. Rev. Lett.* 93:207001
73. Hinkov V, Haug D, Fauqué B, Bourges P, Sidis Y, et al. 2008. *Science* 319:597–600
74. Haug D, Hinkov V, Suchaneck A, Inosov DS, Christensen NB, et al. 2009. *Phys. Rev. Lett.* 103:017001
75. Doiron-Leyraud N, Proust C, LeBoeuf D, Levallois J, Bonnemaison J-B, et al. 2007. *Nature* 447:565–68
76. Jaudet C, Vignolles D, Audouard A, Levallois J, LeBoeuf D, et al. 2008. *Phys. Rev. Lett.* 100:187005
77. Yelland E, Singleton J, Mielke CH, Harrison N, Balakirev FF, et al. 2008. *Phys. Rev. Lett.* 100:047003
78. Bangura AF, Fletcher JD, Carrington A, Levallois J, Nardone M, et al. 2008. *Phys. Rev. Lett.* 100:047004
79. Audouard A, Jaudet C, Vignolles D, Liang R, Bonn DA, et al. 2009. *Phys. Rev. Lett.* 103:157003
80. Chakravarty S. 2008. *Science* 319:735–36
81. Liang R, Bonn DA, Hardy WN. 2006. *Phys. Rev. B* 73:180505
82. Segawa K, Ando Y. 2004. *Phys. Rev. B* 69:104521
83. Ito T, Takenaka K, Uchida S. 1993. *Phys. Rev. Lett.* 70:3995–98
84. Kivelson SA, Fradkin E, Emery VJ. 1998. *Nature* 393:550–53
85. Behnia K. 2009. *J. Phys. Condens. Matter* 21:113101
86. Matusiak M, Naqib SH, Kokanović I, Cooper JR. 2009. *Europhys. Lett.* 86:17005
87. Daou R, Chang J, LeBoeuf D, Cyr-Choinière O, Laliberté F, et al. 2010. *Nature* 463:519–22
88. Wang Y, Li P, Ong NP. 2006. *Phys. Rev. B* 73:024510
89. Ando Y, Segawa K, Komiya S, Lavrov AN. 2002. *Phys. Rev. Lett.* 88:137005
90. Harris R, Turner PJ, Kamal S, Hosseini AR, Dosanjh P, et al. 2006. *Phys. Rev. B* 74:104508
91. Kohsaka Y, Taylor C, Wahl P, Schmidt A, Lee J, et al. 2008. *Nature* 454:1072–78
92. Armitage NP, Fournier P, Greene RL. 2010. *Rev. Mod. Phys.* In press
93. Dagan Y, Qazilbash MM, Hill CP, Kulkarni VN, Greene RL. 2004. *Phys. Rev. Lett.* 92:167001
94. Armitage NP, Ronning F, Lu DH, Kim C, Damascelli A, et al. 2002. *Phys. Rev. Lett.* 88:257001
95. Helm T, Kartsovnik MV, Bartkowiak M, Bittner N, Lambacher M, et al. 2009. *Phys. Rev. Lett.* 103:157002
96. Lin J, Millis AJ. 2005. *Phys. Rev. B* 72:214506
97. Motoyama EM, Yu G, Vishik IM, Vajk OP, Mang PK, Greven M. 2007. *Nature* 445:186–89
98. Kyung B, Hankevych V, Daré A-M, Tremblay A-MS. 2004. *Phys. Rev. Lett.* 93:147004
99. Fournier P, Mohanty P, Maiser E, Darzens S, Venkatesan T, et al. 1998. *Phys. Rev. Lett.* 81:4720–23

85. Presents a recent survey of the Nernst effect in metals.

Annual Review of Condensed Matter Physics

Volume 1, 2010

Contents

Errata

An online log of corrections to *Annual Review of Condensed Matter Physics* articles may be found at http://conmatphys.annualreviews.org/errata.shtml